ELSEVIER

Journal of Molecular Catalysis A: Chemical 169 (2001) 295–301

JOURNAL OF MOLECULAR CATALYSIS A: CHEMICAL

www.elsevier.com/locate/molcata

Amorphous Ni-B/γ-Al_2O_3 catalyst prepared in a modified drying approach and its excellent activity in benzene hydrogenation

Jiang Li, Minghua Qiao, Jing-fa Deng*

Department of Chemistry, Fudan University, Shanghai 200433, PR China

Received 16 December 2000; accepted 6 January 2001

Abstract

A two-step dying approach was proposed for the preparation of supported amorphous Ni-B/γ-Al_2O_3 catalyst. After wetness impregnation of $NiCl_2$ aqueous solution, the catalyst precursor was dried at 343 K first, followed by drying at 383 K before KBH_4 reduction (denoted as Ni-B/γ-Al_2O_3 (LT)). For comparison, the precursor was directly dried at 383 K and reduced by KBH_4 (denoted as Ni-B/γ-Al_2O_3 (HT)). Liquid phase hydrogenation of benzene to cyclohexane was employed as the probe reaction. While X-ray diffraction (XRD), extended X-ray absorption fine structure (EXAFS), X-ray photoelectron spectroscopy (XPS) and turnover frequency (TOF) revealed no considerable electronic or structural difference between the active components of these two catalysts, scanning electron micrography (SEM), H_2 chemisorption and XPS intensity analysis demonstrated the higher dispersion of active component in the Ni-B/γ-Al_2O_3 catalyst prepared by the two-step drying approach, which can account for the superior catalytic performance of Ni-B/γ-Al_2O_3 (LT) to Ni-B/γ-Al_2O_3 (HT) in benzene hydrogenation.

Keywords: Ni-B/γ-Al_2O_3; Amorphous alloy; High dispersion; Benzene hydrogenation; Preparation

1. Introduction

Hydrogenation of aromatic hydrocarbons to saturated cyclic products is of current interest due to the environmental consideration and the wide range of industrial process [1]. On the one hand, cyclohexane, the precursor for nylon-6 and nylon-66, is mainly derived from benzene hydrogenation, and phenol and cyclohexylamine can be synthesized in the cyclohexane route. On the other hand, the existence of excessive amount of aromatics in kerosene can lead to serious air pollution [2]. So many metal catalysts have been studied for benzene hydrogenation [3–13].

Recently, amorphous metal alloys have gained much attention as promising novel catalytic materials [14–16]. Their unique isotropic structure and high concentration of co-ordinatively unsaturated sites [17,18] lead to superior catalytic activity and selectivity to their crystalline counterparts. However, the amorphous alloys prepared by either the quenching method or chemical reduction show low thermal stability [19], which severely restricts their application in industry. In order to overcome the shortcoming while retaining their attractive characteristics, supported amorphous alloys were prepared and remarkable improvement in the crystallization temperature (T_c) was reported. Furthermore, the dispersion of the active sites was also enhanced [19]. Most of the supported amorphous catalysts reported so far have been prepared by wet impregnation of metal

* Corresponding author. Tel: +86-21-65643977; fax: +86-21-65641740.
E-mail address: jfdeng@srcap.stc.sh.cn (J.-f. Deng).

1381-1169/01/$ – see front matter
PII: S1381-1169(01)00048-6

salts and directly dried at 383 K. And no attempt has been made to influence drying condition on the activity of the resulting amorphous catalyst. In this paper, we modified the drying process and a two-step drying approach was proposed in the preparation of amorphous Ni-B/γ-Al_2O_3 catalyst. The higher dispersion of the active component and subsequently the superior benzene hydrogenation performance were identified.

2. Experimental

2.1. Catalyst preparation

A series of Ni-B/γ-Al_2O_3 samples were prepared by the following procedure. Pre-dried γ-Al_2O_3 (40–60 mesh, 197 $m^2\,g^{-1}$) was impregnated with a desired amount of $NiCl_2$ aqueous solution. Then it was dried at 343 K with gentle stirring, followed by drying at 383 K overnight to exclude residual water. The precursor was reduced by adding 2 M KBH_4 solution containing 0.20 M NaOH, during which the mixture was vigorously stirred. The molar ratio of B/Ni was adjust to 3/1 to ensure that all the nickel cations on the support were reduced. The resulting Ni-B/γ-Al_2O_3 catalyst was washed with distilled water until its pH value was about 7 and then kept in ethanol absolute for future use.

For comparison, the Ni-B/γ-Al_2O_3 sample was prepared by the similar method as mentioned above. The only difference was that the precursor was directly dried at 383 K overnight after impregnation. According to their different drying approaches, the former was denoted as Ni-B/γ-Al_2O_3 (LT) and the latter as Ni-B/γ-Al_2O_3 (HT).

The Ni/γ-Al_2O_3 catalyst was prepared in the way depicted in [10].

2.2. Chemical analysis and characterization

The compositions of the supported Ni-B samples were analyzed by inductively coupled plasma method (ICP). BET surface areas were measured by N_2 adsorption at 77 K on a Micromeritics ASAP-2000 adsorption apparatus. The in situ X-ray diffraction (XRD) patterns under H_2 atmosphere were obtained on a Bruker D8 advance X-ray powder diffractometer using Ni-filtered Cu Kα radiation (0.15418 nm). The sample was held at a certain temperature for 0.5 h, then cooled down to room temperature before collecting the XRD data. Extended X-ray absorption fine structure (EXAFS) of the samples was measured on 4W1B in Beijing Synchrotron Radiation Facility, China. The radial distribution functions (RDF) of the samples were obtained from the $\chi(k)k^3$ by the fast Fourier transformation. Differential scanning calorimetry (DSC) was conducted on a Perkin-Elmer DSC under high purity N_2 (99.999%) atmosphere at a heating rate of 5 K min^{-1}. The surface morphology was observed by scanning electron micrography (SEM) on a JEOL JSM-840 scanning electron microscope. X-ray photoelectron spectroscopy (XPS) spectra were recorded on a Perkin-Elmer PHI 5000C ESCA system with Al Kα X-ray excitation source ($h\nu = 1486.6$ eV). All the binding energies (BE) were referenced to the C 1s peak of contaminant carbon at 284.6 eV with an uncertainty of ±0.2 eV. H_2 chemisorption was carried out with a pulsed method [20] at room temperature on a Micromeritics 2900 TPR/TPD apparatus. The number of surface metal active sites was calculated by assuming H/Ni = 1 [21]. Before the measurements, all the samples were treated in situ in an Ar flow of 30 ml min^{-1} at 473 K for 2 h to clean the surface.

2.3. Activity measurements

The liquid-phase hydrogenation of benzene to cyclohexane was carried out in a 500 ml stainless steel autoclave with a mechanical stirrer. After 1 g of catalyst and 200 ml of benzene were introduced into the autoclave, it was sealed and purged with H_2 for four times to remove air. The hydrogenation was carried out at a certain temperature and H_2 pressure with a stirring rate of 1000 rpm to exclude mass transfer limit. The reaction was monitored by sampling the reaction mixture at constant intervals, followed by gas chromatographic analysis with a TCD detector. No products other than cyclohexane were detected. Turnover frequency (TOF) was expressed as the number of benzene molecules converted per second per surface active nickel atom [10]. The TOF values listed below were obtained in at least three independent experiments. It is found that the experimental error was within 10%.

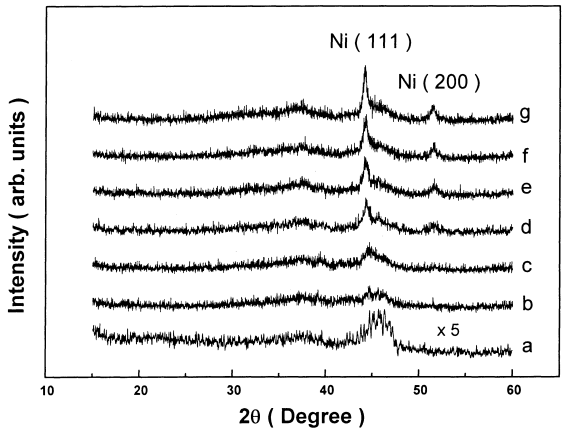

Fig. 1. In situ XRD patterns of Ni-B/γ-Al_2O_3 (LT) sample at (a) 300 K; (b) 500 K; (c) 550 K; (d) 600 K; (e) 650 K; (f) 700 K; (g) 800 K.

3. Results and discussion

3.1. Characterization of the samples

Fig. 1 shows XRD patterns of 9.6 wt.% Ni-B/γ-Al_2O_3 (LT) sample heated from 300 to 800 K under H_2 atmosphere. From room temperature to about 550 K, only a broad peak around $2\theta = 46^\circ$ was observed due to the amorphous nature of the as-prepared sample [16], which was further verified by EXAFS showing only the first-near-neighbor atom layer (Fig. 2), illustrating the long-range disordering character of

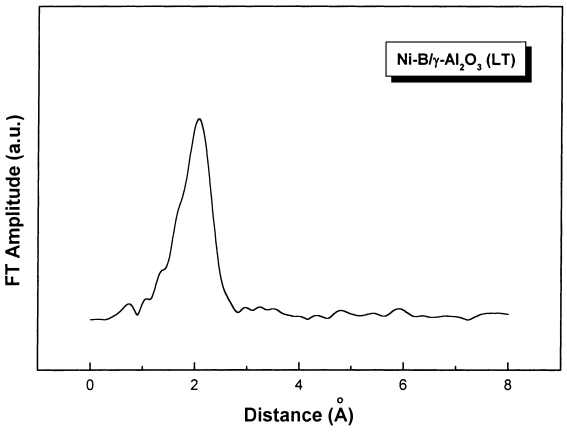

Fig. 2. RDF curve of Ni K-edge of the freshly prepared Ni-B/γ-Al_2O_3 (LT).

the amorphous alloys. At higher temperatures, some diffraction peaks appeared, as shown in Fig. 1d–g, indicative of the occurrence of crystallization. Only diffraction lines of Ni(1 1 1) and Ni(2 0 0) were observed in the XRD patterns, implying phase separation and crystallization of the amorphous Ni–B alloy. The absence of features related to boron when the sample was crystallized is ascribed to its low concentration and high dispersion on the support [22].

The thermal stability of 7.1, 11.8 wt.% Ni-B/γ-Al_2O_3 (LT) and 10.1 wt.% Ni-B/γ-Al_2O_3 (HT) samples was investigated by DSC. From Fig. 3, one can conclude that (1) the thermal stability of Ni-B/γ-Al_2O_3 (LT) is higher than Ni-B/γ-Al_2O_3 (HT); and (2) the thermal stability of Ni-B/γ-Al_2O_3 (LT) decreases with increasing Ni loading. For unsupported amorphous Ni–B alloy, crystallization begins at 417.1 K [23], at least 250 K lower than the supported counterpart. It is understandable that support can inhibit the aggregation of surface components, which is the pre-requisite for crystallization, by its interaction with surface components. As the support and the surface component are the same in the present case, the higher thermal stability of Ni-B/γ-Al_2O_3 (LT) than that of Ni-B/γ-Al_2O_3 (HT) and the higher thermal stability of Ni-B/γ-Al_2O_3 (LT) at lower Ni loading than that at higher Ni loading can be ascribed to the higher dispersion of Ni–B alloy on the surface, which maximizes the interaction between Ni–B alloy and γ-Al_2O_3. This suggestion is further supported by H_2 chemisorption and XPS intensity analysis shown later. On the other hand, the lower crystallization temperature revealed by in situ XRD than DSC is due to the longer holding time at a certain temperature for in situ XRD.

Fig. 4 shows the SEM morphologies of the freshly prepared 9.6 wt.% Ni-B/γ-Al_2O_3 (LT) and 10.1 wt.% Ni-B/γ-Al_2O_3 (HT) samples. Both samples displayed cotton-like morphology, consistent with other Ni-based amorphous alloy samples [19]. It is also observed that although with similar nickel loading, the Ni–B alloy particles in Ni-B/γ-Al_2O_3 (LT) were homogeneously dispersed (Fig. 4a), while for Ni-B/γ-Al_2O_3 (HT) some clustering of the active components occurred (Fig. 4b).

The XPS spectra of the freshly prepared 9.6 wt.% Ni-B/γ-Al_2O_3 (LT) sample are shown in Fig. 5. As can be seen from the Ni $2p_{3/2}$ spectra (Fig. 5a), there are indicative peaks of metallic nickel and oxidized

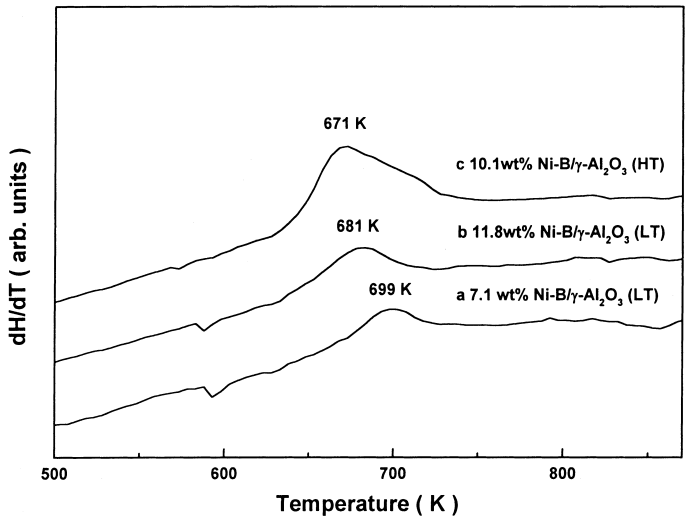

Fig. 3. DSC curves of (a) 7.1 wt.% Ni-B/γ-Al_2O_3 (LT); (b) 11.8 wt.% Ni-B/γ-Al_2O_3 (LT); (c) 10.1 wt.% Ni-B/γ-Al_2O_3 (HT) samples.

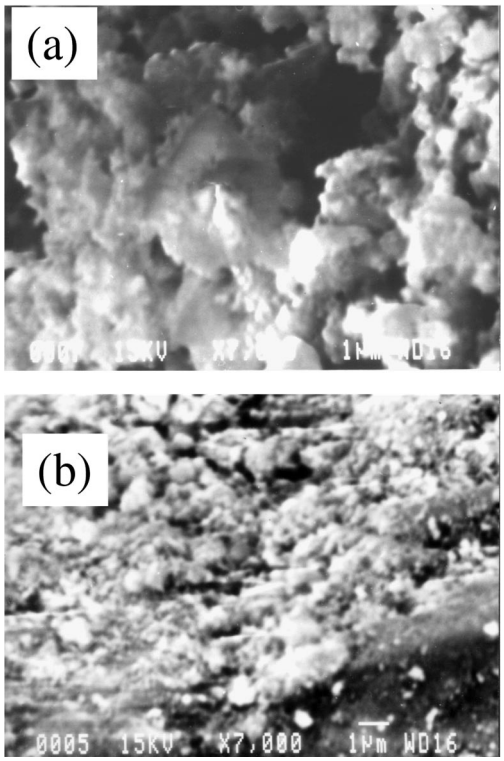

Fig. 4. SEM micrographs of the freshly prepared (a) 9.6 wt.% Ni-B/γ-Al_2O_3 (LT); (b) 10.1 wt.% Ni-B/γ-Al_2O_3 (HT).

nickel at 853 and 856.4 eV, respectively [24]. After Ar^+ sputtering for 15 min, only metallic nickel can be observed. The B 1s level in Fig. 5b demonstrates that boron species are in the elemental and the oxidized states with BE at 188.2 and 192.2 eV, respectively [25]. Different from the Ni $2p_{3/2}$ level, the oxidized boron species were still visible after Ar^+ sputtering. It is generally acknowledged that when using borohydride or hypophosphite as reducing agent, three independent reactions will occur: the hydrolysis of the reducing agent, the reduction of the metal ion, and the reduction of the metalloid. Chen found that when preparing Fe–B, about 50% of KBH_4 were hydrolyzed to boron oxide, which is inevitable for the reaction carried out in aqueous solution [26].

It is worth noting that although no significant BE shift of metallic nickel was observed, the BE of elemental boron shifted about +1.1 eV relative to pure boron [25]. Based on their XPS measurements, Okamoto and co-workers claimed that in amorphous Ni–B alloy boron donates electrons to the alloying nickel [27,28]. Therefore, boron is electron-deficient while nickel is electron-rich in the amorphous Ni–B alloy. The charge transfer verifies the bonding between nickel and boron in the amorphous alloy, leading to smaller Ni–B atomic distance, obtained by measuring the Ni K-edge EXAFS spectra [29], than the sum of Goldschmidt radii of individual

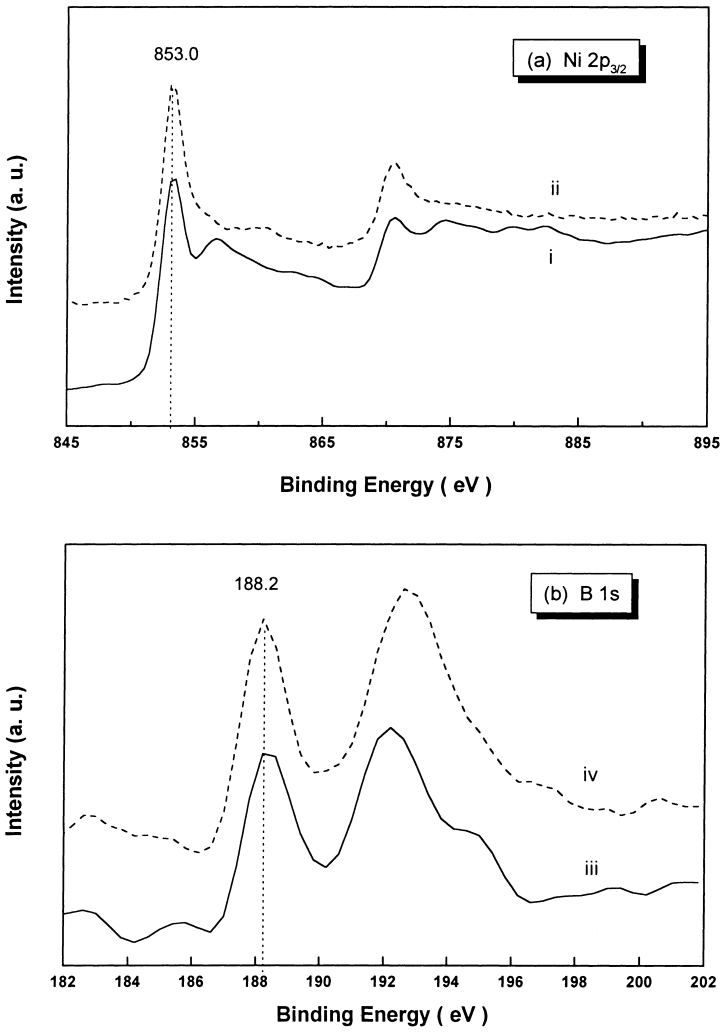

Fig. 5. (a) Ni $2p_{3/2}$; (b) B 1s XPS spectra of Ni-B/γ-Al_2O_3 (LT) sample. The curves (i) and (iii) are of the as-prepared sample; (ii) and (iv) are of the sample after Ar^+ sputtering for 15 min.

atoms. We did not observe the BE shift of nickel alloying with boron, which can be justified by the following argument. From Ni^0 to Ni^{2+}, the Ni 2p BE shift is about +1 eV, while from B^0 to B^{3+}, the B 1s BE shift is about +6 eV. By considering the B 1s BE shift of +1.1 eV in Ni-B/γ-Al_2O_3, combined with the bulk composition of $\sim Ni_{63}B_{37}$ (Table 1), a rough estimation gave a Ni 2p BE shift of −0.11 eV ($\Delta BE = -(1.1 \times 0.37)/(6 \times 0.63)$) in amorphous Ni–B alloy, which is well within the experimental error of ±0.2 eV.

3.2. Correlation of activity of the Ni-B/γ-Al_2O_3 (LT) catalyst with its structure

Table 1 lists Ni/B atomic ratio, BET surface area, number of surface active nickel atoms, and TOF of benzene over Ni-B/γ-Al_2O_3 (LT) catalysts with different Ni loading. No significant change in the composition of Ni–B alloy was observed, showing that the reduction of nickel cations by KBH_4 was proceeded quantitatively. The decrease in BET surface area with the increase of Ni loading is mainly due to the block of

Table 1
Activity of benzene hydrogenation over Ni-B/γ-Al_2O_3 (LT) catalysts

Ni loading (wt.%)	Bulk composition (atomic ratio)	S_{BET} ($m^2\,g^{-1}$)	Pore diameter (nm)	Number of active Ni atoms[a] ($10^{19}\,g_{cat}^{-1}$)	TOF[b] (s^{-1})
2.4	$Ni_{64}B_{36}$	170.5	10.7	0.61	1.52
5.6	$Ni_{64}B_{36}$	163.1	10.2	1.78	1.50
7.1	$Ni_{62}B_{38}$	160.3	9.9	2.39	1.54
9.6	$Ni_{63}B_{37}$	154.1	9.5	3.75	1.60
11.8	$Ni_{62}B_{38}$	150.5	9.1	3.94	1.60

[a] Measured by H_2 chemisorption.
[b] Reaction condition: 200 ml of benzene, 1 g of Ni-B/γ-Al_2O_3 (LT), reaction temperature 373 K, hydrogen pressure 4 MPa.

Table 2
Comparison of hydrogenation activities over Ni-based catalysts

Catalyst	Ni loading (wt.%)	Number of active Ni atoms ($10^{19}\,g_{cat}^{-1}$)	TOF (s^{-1})	Conversion of benzene[a] (%)
Ni/γ-Al_2O_3	10	0.79	1.49	18.7
Ni-B/γ-Al_2O_3 (HT)	10.1	2.89	1.50	68.8
Ni-B/γ-Al_2O_3 (LT)	9.6	3.75	1.60	95.2

[a] The reaction condition is the same as those in Table 1. Reaction time: 6 h.

the pores in γ-Al_2O_3 by Ni–B alloy particles, which is confirmed by the decrease of pore diameters. From the increasing number of active nickel atoms and the marginal difference in the TOF values, it is concluded that for the amorphous Ni-B/γ-Al_2O_3 (LT) catalysts with different Ni loading, the dispersion of Ni active sites plays a key role in determining the activity.

Table 2 lists the number of active nickel atoms, TOF values and conversions of benzene over Ni-B/γ-Al_2O_3 (LT), Ni-B/γ-Al_2O_3 (HT) and Ni/γ-Al_2O_3 catalysts with similar Ni loading. Though the Ni loadings were similar, the number of active nickel atoms of the Ni-B/γ-Al_2O_3 (LT) and Ni-B/γ-Al_2O_3 (HT) catalysts were 3.7 and 2.6 times higher than that of the Ni/γ-Al_2O_3 catalyst. Accordingly, the benzene conversions in 6 h under the same reaction condition were 95.2, 68.8 and 18.7% for Ni-B/γ-Al_2O_3 (LT), Ni-B/γ-Al_2O_3 (HT) and Ni/γ-Al_2O_3, respectively.

The difference is worth noting between the number of active sites of Ni-B/γ-Al_2O_3 (LT) and Ni-B/γ-Al_2O_3 (HT) catalysts even though they have the same active components and support. It seems that the drying method is essential in determining the distribution of the Ni cations on the support and hence the dispersion of surface active nickel atoms over the catalyst after reduction. We have shown by SEM that Ni dispersed homogeneously in the Ni-B/γ-Al_2O_3 (LT) catalyst, while for Ni-B/γ-Al_2O_3 (HT) some clustering occurred. DSC implied the stronger interaction between Ni–B alloy and the support due to the maximization of its contact with the support. Much direct evidence was provided by XPS intensity analysis. We have calculated the Ni $2p_{3/2}$/Al 1s intensity ratios between these two catalysts after fitting the Ni $2p_{3/2}$ and Al 1s peaks with a Voigt function when supposing a linear background. It is found that the Ni $2p_{3/2}$/Al 1s intensity ratio for Ni-B/γ-Al_2O_3 (LT) is 1.32 times of that for Ni-B/γ-Al_2O_3 (HT), lending further support to our suggestion.

4. Conclusions

A novel amorphous Ni-B/γ-Al_2O_3 (LT) catalyst was prepared by a two-step drying approach before chemical reduction by KBH_4. Its superior catalytic activity to that of Ni-B/γ-Al_2O_3 (HT) or Ni/γ-Al_2O_3 catalysts was identified in liquid phase hydrogenation of benzene to cyclohexane. DSC and in situ XRD revealed the higher thermal stability of Ni-B/γ-Al_2O_3 (LT) than Ni-B/γ-Al_2O_3 (HT), attributable to the stronger interaction between the active components

and γ-Al_2O_3 resulted from the two-step drying approach. The stronger interaction led to higher dispersion of the active components on Ni-B/γ-Al_2O_3 (LT), as confirmed by SEM, H_2 chemisorption and XPS intensity analysis.

Acknowledgements

This work is supported by the Shanghai Research Center of Advanced Materials, the Special Foundation for Doctor Candidate of the State Education Commission of PR China, the National Natural Science Foundation of China, and the SINOPEC.

References

[1] A. Louloudi, N. Papayannakos, Appl. Catal. A 175 (1998) 21.
[2] A. Stanislaus, B.H. Cooper, Catal. Rev. Sci. Eng. 36 (1994) 75.
[3] A.F. Flores, J.R.L. Burwell, J.B. Butt, J. Chem. Soc., Faraday Trans. 88 (1992) 1191.
[4] S.D. Lin, M.A. Vannice, J. Catal. 143 (1993) 539.
[5] K.K.A. Rashid, K.V. Lakshmi, M. Nandan, K.O. Xavier, B. Sen, Stud. Surf. Sci. Catal. 113 (1998) 829.
[6] P. Chou, M.A. Vannice, J. Catal. 107 (1987) 140.
[7] C.A. Koh, R. Nooney, S. Tahir, Catal. Lett. 47 (1997) 199.
[8] M.C. Schoenmaker-Stolk, J.W. Verwijs, J.A. Don, J.J.F. Scholten, Appl. Catal. 29 (1987) 73.
[9] P. Badenes, L. Daza, I. Rodriguez-Ramos, A. Guerrero-Ruiz, Stud. Surf. Sci. Catal. 112 (1997) 241.
[10] S. Narayanan, K. Uma, J. Chem. Soc., Faraday Trans. 1 81 (1985) 2733.
[11] S.N. Chaudhuri, S.K. Nath, D.S. Majumdar, Stud. Surf. Sci. Catal. 113 (1998) 793.
[12] K. Hadjiivanov, M. Mihaylov, N. Abadjieva, D. Klissurski, J. Chem. Soc., Faraday Trans. 94 (1998) 3711.
[13] A. Barbier, A. Hanif, J.-A. Dalmon, G.A. Martin, Appl. Catal. A 168 (1998) 333.
[14] T. Katona, A. Molnar, J. Catal. 153 (1995) 333.
[15] K. Hashimoto, Mater. Sci. Eng. A: Struct. 226 (1997) 891.
[16] J.-F. Deng, H.X. Li, W.J. Wang, Catal. Today 51 (1999) 113.
[17] M. Shibata, T. Masumoto, Prep. Catal. 4 (1987) 353.
[18] A. Molnar, G.V. Smith, M. Bartok, Adv. Catal. 36 (1989) 329.
[19] J.-F. Deng, Curr. Top. Catal. 2 (1999) 1.
[20] P.I. Lee, J.A. Schwarz, J. Catal. 73 (1982) 272.
[21] C.H. Bartholomew, R.B. Pannell, J. Catal. 65 (1980) 390.
[22] Y.C. Xie, Y.Q. Tang, Adv. Catal. 37 (1990) 1.
[23] J.-F. Deng, J. Yang, S.S. Sheng, H.R. Chen, G.X. Xiong, J. Catal. 150 (1995) 434.
[24] Handbook of X-ray Photoelectron Spectroscopy, Perkin Elmer, Eden Praine, 1992.
[25] H. Li, H.X. Li, W.L. Dai, W.J. Wang, Z.G. Fang, J.-F. Deng, Appl. Surf. Sci. 152 (1999) 25.
[26] Y. Chen, Catal. Today 44 (1998) 3.
[27] Y. Okamoto, Y. Nitta, T. Imanaka, S. Teranishi, J. Chem. Soc., Faraday Trans. 15 (1979) 2027.
[28] Y. Okamoto, Y. Nitta, T. Imanaka, S. Teranishi, J. Catal. 64 (1980) 397.
[29] L. Finney, Nature 266 (1977) 309.